



Ocean alkalinity enhancement using sodium carbonate salts does not lead to measurable changes in Fe dynamics in a mesocosm experiment

David González-Santana¹, María Segovia², Melchor González-Dávila¹, Librada Ramírez², Aridane G. González¹, Leonardo J. Pozzo-Pirotta², Veronica Arnone¹, Victor Vázquez², Ulf Riebesell³, and J. Magdalena Santana-Casiano¹

¹Instituto de Oceanografía y Cambio Global, IOCG, Universidad de Las Palmas de Gran Canaria, ULPGC, Las Palmas de Gran Canaria, Spain

²Department of Ecology, Faculty of Sciences, University of Málaga, Málaga, Spain

³GEOMAR Helmholtz Centre for Ocean Research Kiel, Kiel, Germany

Correspondence: David González-Santana (david.gonzalez@fpct.ulpgc.es)

Received: 30 November 2023 – Discussion started: 11 December 2023

Revised: 21 March 2024 – Accepted: 25 March 2024 – Published: 5 June 2024

Abstract. The addition of carbonate minerals to seawater through an artificial ocean alkalinity enhancement (OAE) process increases the concentrations of hydroxide, bicarbonate, and carbonate ions. This leads to changes in the pH and the buffering capacity of the seawater. Consequently, OAE could have relevant effects on marine organisms and in the speciation and concentration of trace metals that are essential for their physiology. During September and October 2021, a mesocosm experiment was carried out in the coastal waters of Gran Canaria (Spain), consisting on the controlled variation of total alkalinity (TA). Different concentrations of carbonate salts (NaHCO_3 and Na_2CO_3) previously homogenized were added to each mesocosm to achieve an alkalinity gradient between $\Delta 0$ to $\Delta 2400 \mu\text{mol L}^{-1}$. The lowest point of the gradient was $2400 \mu\text{mol kg}^{-1}$, being the natural alkalinity of the medium, and the highest point was $4800 \mu\text{mol kg}^{-1}$. Iron (Fe) speciation was monitored during this experiment to analyse total dissolved iron (TdFe, unfiltered samples), dissolved iron (dFe, filtered through a $0.2 \mu\text{m}$ pore size filter), soluble iron (sFe, filtered through a $0.02 \mu\text{m}$ pore size filter), dissolved labile iron (dFe'), iron-binding ligands (LFe), and their conditional stability constants (K'_{FeL}) because of change due to OAE and the experimental conditions in each mesocosm. Observed iron concentrations were within the expected range for coastal waters, with no significant increases due to OAE. However, there were variations in Fe size fractionation during the ex-

periment. This could potentially be due to chemical changes caused by OAE, but such an effect is masked by the stronger biological interactions. In terms of size fractionation, sFe was below 1.0 nmol L^{-1} , dFe concentrations were within $0.5\text{--}4.0 \text{ nmol L}^{-1}$, and TdFe was within $1.5\text{--}7.5 \text{ nmol L}^{-1}$. Our results show that over 99 % of Fe was complexed, mainly by L_1 and L_2 ligands with k'_{FeL} ranging between 10.92 ± 0.11 and 12.68 ± 0.32 , with LFe ranging from 1.51 ± 0.18 to $12.3 \pm 1.8 \text{ nmol L}^{-1}$. Our data on iron size fractionation, concentration, and iron-binding ligands substantiate that the introduction of sodium salts in this mesocosm experiment did not modify iron dynamics. As a consequence, phytoplankton remained unaffected by alterations in this crucial element.

1 Introduction

Artificial ocean alkalinity enhancement (OAE) can lead to the atmospheric carbon dioxide removal (CDR) by increasing the ocean carbon uptake and reversing ocean acidification (OA), favouring a higher ocean pH buffering capacity (Kheshgi, 1995; Renforth and Henderson, 2017; Lenton et al., 2018). OAE can be likened to an acceleration of natural chemical weathering processes of minerals. Weathering reactions have played a role in modulating climate on geological timescales (Zeebe, 2012; Colbourn et al., 2015).

OAE has consequences for the CO₂–carbonate system in the ocean. The increase in ocean alkalinity raises both total dissolved inorganic carbon (DIC) and pH, subsequently increasing the carbonate ion concentration, as well as decreasing *p*CO₂. This increases the *p*CO₂ imbalance between the ocean and atmosphere, leading to an enhancement of ocean carbon uptake. The artificial augmentation of alkalinity could also have consequences for marine ecosystems, both for the biota and for the chemical constituents of seawater, including elements that are essential for the ecosystem (Feng et al., 2016). The consumption of atmospheric CO₂ and pH increase during OAE may be accompanied by changes in the release of mineral dissolution products such as Si, Ca, Mg, Fe, or Ni. The ecological and biogeochemical consequences of OAE will also depend on the minerals used during alkalization (e.g. Mg₂SiO₄, CaO, Na₂CO₃) (Renforth and Henderson, 2017; Hartmann et al., 2013; Bach et al., 2019). Hence, it is necessary to perform experiments that may support or dissuade the use and viability of this technique under different experimental conditions. One controlled, i.e. semi-natural, way to perform these types of experiments is by using mesocosms. Mesocosm studies allow rigorous testing of marine carbon dioxide removal techniques (mCDR) at the ecosystem level since the only variable that is artificially modified is the variable of interest (OAE), allowing the enclosed water column to maintain its chemical and biological properties.

OAE could have an impact on trace metals that are essential for marine organisms, and this effect has been scarcely investigated so far (Guo et al., 2022; Xin et al., 2023). Among metals, Fe is the most essential micronutrient controlling phytoplankton growth mainly through nitrate assimilation and photosynthesis (Behrenfeld and Milligan, 2013). Thus, the growth and development of marine phytoplankton is linked to the biogeochemical cycling of Fe (Jickells et al., 2005; Moore et al., 2001), by regulating both the structure and the productivity of marine ecosystems (Tagliabue et al., 2017; Boyd and Ellwood, 2010).

The assimilation of iron by marine organisms is not straightforward. Fe bioavailability, i.e. iron available for uptake, and therefore growth, is controlled by many factors. It depends on the different forms (chemical speciation) in which iron is found in solution (Sutak et al., 2020). Indeed, not all iron species are bioavailable, only those in the dissolved (dFe) phase. Under oxygenated ocean conditions, the most abundant form of iron is the insoluble form of oxidized iron, Fe(III). pH is the main variable that controls Fe speciation in this condition. Fe(II) is thermodynamically unstable and oxidized on timescales of minutes to hours (Santana-Casiano et al., 2005; González-Santana et al., 2021). Higher pH alters iron speciation, decreases Fe solubility and Fe(II) half-life, and thus decreases dissolved iron (dFe) concentrations (Liu and Millero, 2002; Boye et al., 2006; González-Dávila et al., 2006). However, there are several factors that can significantly alter and control iron speci-

ation, such as photooxidation in surface waters, the presence of organic ligands (*L*), and the decreasing oxygen concentration (Santana-Casiano et al., 2022; González et al., 2019; Benner, 2011; Barbeau, 2006; Moffett, 2021; Hopkinson and Barbeau, 2007). All of these factors can induce a reduction of Fe(III) to Fe(II) depending on the conditions and characteristics of the organic compounds involved. Moreover, organic matter plays an essential role, because it can complex up to 99 % of the iron (Fe(III)-*L*) forming part of the dFe (Wu and Luther III, 1994; Arnone et al., 2022). The concentration and strength of iron-binding organic ligands (*L*_{Fe}) modulate Fe speciation and its bioavailability. In addition, particle size (physical speciation) is key for Fe cycling, since the colloidal size fraction remains in solution while larger fractions tend to sink down, being excluded from the system. All these processes were demonstrated during a mesocosm experiment, in a Norwegian fjord, that studied the effects of ocean acidification. In this experiment, both low pH and strong organic ligands enhanced the solubility of particulate and colloidal Fe (Segovia et al., 2017; Lorenzo et al., 2020). This promoted significantly higher Fe availability to phytoplankton, directly impacting on their physiology and controlling the phytoplankton community structure in coastal ecosystems (Segovia et al., 2017; Lorenzo et al., 2020; Mausz et al., 2020).

The introduction of carbonate minerals into seawater for OAE (Bach et al., 2019) is expected to increase the concentrations of hydroxide, bicarbonate, and carbonate (OH⁻, HCO₃⁻ and CO₃²⁻). This will change metal ion speciation in seawater (Millero et al., 2009). Metals that form complexes with OH⁻ and CO₃²⁻, such as Fe, may be less abundant in their free forms at higher pH. Moreover, Fe(II) oxidation rate constants are strongly increased under high HCO₃⁻ and CO₃²⁻ concentrations (Santana-Casiano et al., 2005, 2006), making Fe less bioavailable. OAE can also cause a release of Ca²⁺ or Mg²⁺ ions (Bach et al., 2019). These ions compete with Fe for specific functional groups of the organic ligand, which would affect the redox speciation of this metal (Santana-Casiano et al., 2010).

In this sense, the impact of OAE on the iron cycle could be that the Fe speciation will change with enhanced alkalinity. In the presence of organic compounds produced by the organisms in the mesocosms, the formation of strong organic complexes (FeL) will dominate the speciation of Fe. The Ca²⁺ or Mg²⁺ ions produced in OAE if Mg₂SiO₄ or CaO were used could compete with Fe for the organic ligands, which would affect the Fe redox speciation and the bioavailability. To avoid this effect, alkalization with NaHCO₃ and Na₂CO₃ is recommended.

The aim of this research was to study the evolution of inorganic and organic Fe speciation in seawater under OAE scenarios. We considered whether the added material acted as a significant iron source and its effects on both the iron size fractionation and Fe-binding ligand evolution.

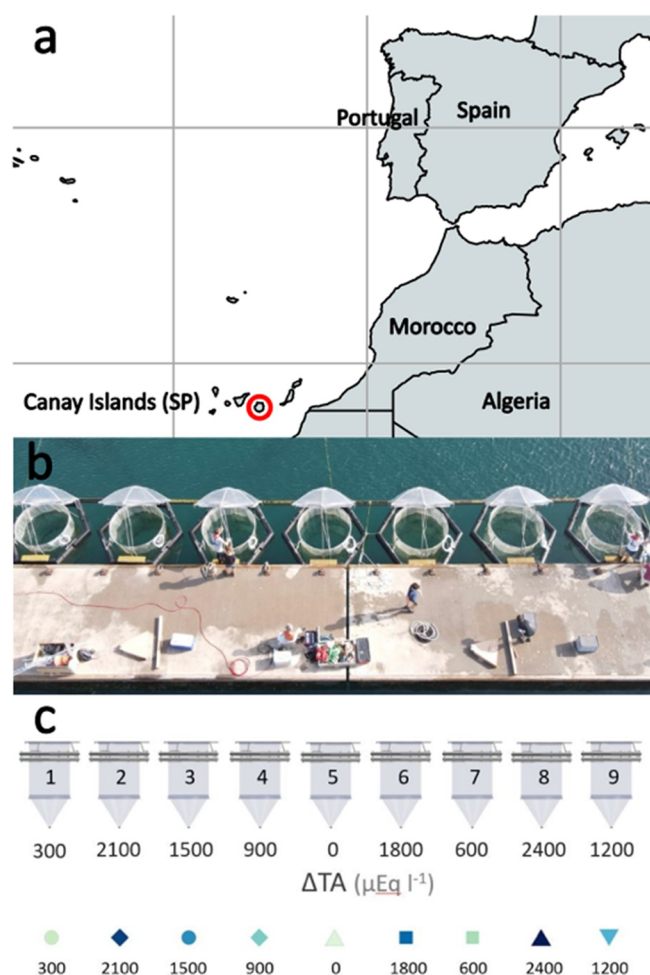


Figure 1. Study site. (a) Location in the Gran Canaria port town of Taliarte, Spain (©Google Earth Pro); (b) operating mesocosms during the experiment (photograph by Peter Yeung, National Geographic©); (c) mesocosm experimental design representing the alkalinity gradient (OAE) ($\mu\text{mol L}^{-1}$) in the nine mesocosms: M5 (0), M1 (300), M7 (600), M4 (900), M9 (1200), M3 (1500), M6 (1800), M2 (2100), and M8 (2400) (design by Silvan Goldenberg, GEOMAR©).

2 Material and methods

2.1 Mesocosms experimental design and distribution

The mesocosm experiment was conducted in the port of Taliarte, Telde, Gran Canaria, during a 33 d period from September to October 2021. Nine mesocosms (M1–M9) were deployed in the port of Taliarte containing a natural seawater column of 8.3 m^3 each at 5 m depth, with a sediment trap attached to the bottom of the bag (Riebesell et al., 2013; Taucher et al., 2017) (Fig. 1).

Mesocosms were set up on 10 September 2021 (day t0). Phase 0 (t1–t3) was established at the beginning of the experiment, prior to the addition of the sodium carbonate salts

(NaHCO_3 and Na_2CO_3), to analyse the conditions of the mesocosms before their alkalization. On day 4 (t4) of the experiment, 40 L of natural seawater with different concentrations of carbonate salts (NaHCO_3 and Na_2CO_3) previously homogenized was added to each mesocosm to achieve an alkalinity gradient between $\Delta 0$ (lowest) $\Delta 2400$ (highest) $\mu\text{mol L}^{-1}$. Phase I (t5–t19) began followed by Phase II (t19–t33). Variables were sampled at 1 d intervals. Experimental design represents the alkalinity gradient (OAE) ($\mu\text{mol L}^{-1}$) in the following nine mesocosms: M5 ($\Delta 0$), M1 ($\Delta 300$), M7 ($\Delta 600$), M4 ($\Delta 900$), M9 ($\Delta 1200$), M3 ($\Delta 1500$), M6 ($\Delta 1800$), M2 ($\Delta 2100$), and M8 ($\Delta 2400$) ($\mu\text{mol L}^{-1}$).

2.2 Sampling strategy

Samples were collected in 1 L acid-cleaned LDPE bottles. Trace metal clean (TMC) samples were subsampled from this bottle within an ISO Class-6 laminar flow hood (Cutter et al., 2017). Unfiltered samples (i.e. total dissolved iron, TdFe) were first collected. Aliquots were filtered ($0.2 \mu\text{m}$ Sartobran™ PES) for soluble iron (sFe), dFe, and iron-binding ligands (LFe). Soluble Fe samples were further filtered through acid-cleaned $0.02 \mu\text{m}$ filters (Whatman™ Anotop™ 25/0.02) using a peristaltic pump. The TdFe, dFe, and sFe samples were acidified with HCl ultrapure, 2% v/v to $\text{pH} \sim 1.7$ (Pan-reac) after sampling, and kept in the dark for at least 6 months until analysis. The LFe samples were frozen at -20°C until further analysis was performed.

2.3 Iron concentration analyses

The TdFe, dFe, and sFe samples were analysed in duplicates (two analytical peaks; a second duplicate was performed if the standard deviation was $> 5\%$) using flow injection analysis with chemiluminescence detection (FIA) (Obata et al., 1993; Lohan et al., 2006) inside an ISO Class-6 laminar flow hood inside an ISO Class-5 TMC laboratory. Samples were spiked with 0.013 M ultrapure H_2O_2 (Sigma-Aldrich) 30 min prior to analysis to ensure the complete oxidation of Fe (II) to Fe (III) (Lohan et al., 2006). Each sample was buffered in line to $\text{pH} 3.5$ with 0.15 M ammonium acetate (Supelco and Sigma-Aldrich, SpA) before Fe(III) was pre-concentrated onto the cation exchange resin Toyopearl-AF-Chelate 650 M (Tosohaas) between 60 and 120 s at a flow rate of 1.5 mL min^{-1} . Following a rinse step of weak 0.013 M HCl (Honeywell Fluka™, SpA), Fe was eluted from the resin using 0.24 M HCl (Honeywell Fluka™, SpA) and entered the reaction stream where it was mixed with a 0.015 mM luminol solution containing $70 \mu\text{L L}^{-1}$ triethylenetetramine (Sigma-Aldrich), buffered to $\text{pH} 9.5 \pm 0.1$ using a 1 M ammonia solution (Supelco, SpA). Iron concentrations were quantified using standard additions (TraceCERT) to low Fe seawater. The limit of detection (3 times the standard deviation of the lowest addition) was $0.03 \pm 0.02 \text{ nmol L}^{-1}$, while the precision of three analytical peaks was $< 2\%$. Accu-

racy was established by repeat quantification of dFe in an in-house standard, whose concentration was asserted from the repeat measurement of GSC reference samples yielding $1.59 \pm 0.03 \text{ nmol L}^{-1}$, which agrees with the reported consensus values ($1.54 \pm 0.12 \text{ nmol L}^{-1}$).

2.4 Fe-binding ligands

Iron-binding ligand (L_{Fe}) concentrations and the conditional stability constants ($K_{\text{FeL}}^{\text{cond}}$) were determined by competitive ligand exchange-adsorptive cathodic stripping voltammetry (CLE-ACSV) with ligand competition against TAC (2-(2-thiazolylazo)-*p*-cresol; Sigma-Aldrich). The titration procedure used, established by Croot and Johansson (2000), was carried out with a voltammetric system equipped with a hanging mercury drop electrode (VA663 stand Metrohm), an Ag / AgCl reference electrode with a KCl salt bridge (3 M), and a glassy carbon counter electrode.

Three different reagents were required for titration analysis. A 0.01 M stock solution of TAC as complexing agent was prepared in methanol (Sigma-Aldrich). A buffer of 1 M boric acid in 0.3 M ammonia (pH 8.2), the impurities of which were removed from the solution by the addition of $100 \mu\text{M}$ of MnO_2 , was followed by an overnight stirring and filtration through an acid-cleaned $0.45 \mu\text{m}$ filter (Campos and van den Berg, 1994). Finally, dFe stock solutions were prepared weekly in suprapure HCl. All reagents were stored in the dark and at 8°C when they were not in use.

In the titration method, 10 mL seawater aliquots were pipetted into 12 PTFE vials to which $100 \mu\text{L}$ of boric acid (final concentration 10^{-2} M) and different concentrations of dFe (from 0 to 20 nM) were added immediately. After 1 h of equilibration, $10 \mu\text{L}$ of TAC (final concentration $10 \mu\text{M}$) was added and allowed to equilibrate overnight. Then, for voltammetric analysis, samples were purged with nitrogen gas for 120 s, followed by the application of a deposition potential of -0.41 V for 120 s. After 10 s of equilibration, a differential pulse scan from -0.43 to -0.65 V was applied, with a step potential of 5 mV, modulation amplitude of 20 mV, interval time of 0.091 s, and modulation time of 0.051 s. Finally, the data processing was performed using ProMCC software (Omanović et al., 2015)

3 Results and discussion

The experiment was divided into three distinct phases according to characterized variations in the seawater chemistry and the plankton community development, as indicated above. A Phase 0 was established at the beginning of the experiment (t1–t3) to analyse the conditions in the mesocosms prior to treatment additions (OAE). Phase I (t5–t19) began after alkalization by NaHCO_3 and Na_2CO_3 , and then Phase II followed (t19–t33).

The experimental setup effectively recreated a scenario of ocean liming by establishing a gradient of total alkalinity (TA) increasing in $300 \mu\text{mol L}^{-1}$ intervals. Dissolved inorganic carbon (DIC) and TA were steady until day t21 (Supplement Fig. S1). On that day, in the highest treatment ($\Delta 2400 \mu\text{mol L}^{-1}$), abiotic precipitation occurred, but this event did not have any impact on the phytoplankton community response. A succinct summary of the phytoplankton abundance results is provided next and in Supplement Fig. S2. During Phase I, there was a significant increase in picoeukaryotes abundances at $\Delta 600$, $\Delta 900$, $\Delta 1800$, and $\Delta 2100 \mu\text{mol L}^{-1}$. Additionally, microplankton increased at $\Delta 900 \mu\text{mol L}^{-1}$. In contrast, small nanoeukaryotes ($2\text{--}20 \mu\text{m}$) exhibited a decreasing trend from the experiment's onset, with maximal abundance observed before OAE treatment additions (t1–t3). Moving to Phase II, large nanoeukaryotes ($> 20 \mu\text{m}$) dominated the community, particularly in $\Delta 1500$ and $\Delta 1800 \mu\text{mol L}^{-1}$. Microplankton also increased by the phase's end. *Synechococcus* spp. showed a general increase in cell density over time, peaking at t27 in $\Delta 900 \mu\text{mol L}^{-1}$ but subsequently decreasing in many other treatments. All these data can be consulted for further details and in the articles by Marin-Samper et al. and Ramirez et al. (2024).

3.1 Iron size fractionation

Iron size fractionation (sFe, colloidal iron (cFe), dFe, and TdFe) was determined during the OAE experiment (Fig. 2). The first metal concentration samples were collected on t1 for dFe and sFe, i.e. Phase 0 of the experiment. The initial concentration for dFe was $1.74 \pm 0.44 \text{ nmol L}^{-1}$, ranging from $1.20 \pm 0.02 \text{ nmol L}^{-1}$ at $\Delta 1800$ to $2.39 \pm 0.03 \text{ nmol L}^{-1}$ at $\Delta 1500$. For sFe, the initial concentrations were $0.39 \pm 0.18 \text{ nmol L}^{-1}$, ranging from $0.22 \pm 0.01 \text{ nmol L}^{-1}$ at $\Delta 600$ to $0.74 \pm 0.03 \text{ nmol L}^{-1}$ at $\Delta 1800$.

In the Macaronesia region, dFe concentrations average $0.80 \pm 0.25 \text{ nmol L}^{-1}$ (varying from 0.46 to 1.32 nmol L^{-1}) (Arnone et al., 2022). However, these concentrations are obtained from samples collected on a research vessel using trace metal clean conditions into a trace metal clean bottle following strict trace metal clean conditions (Cutter et al., 2017). As such, t1 dFe concentrations just show a slight increase in dFe when no trace metal clean procedures were followed and mesocosms were kept in the open air but still trying to limit contamination. The observed changes in dFe and sFe concentrations were most likely due to the natural variability between mesocosms. Considering that variability occurs on interannual, seasonal, and diurnal timescales, this also forms part of the system's behaviour (Schulz and Riebesell, 2013). Indeed, considerable natural variability exists in seawater carbonate chemistry speciation, caused by changes in temperature and biological activities such as photosynthesis, respiration, nutrient utilization, remineralization, and cal-

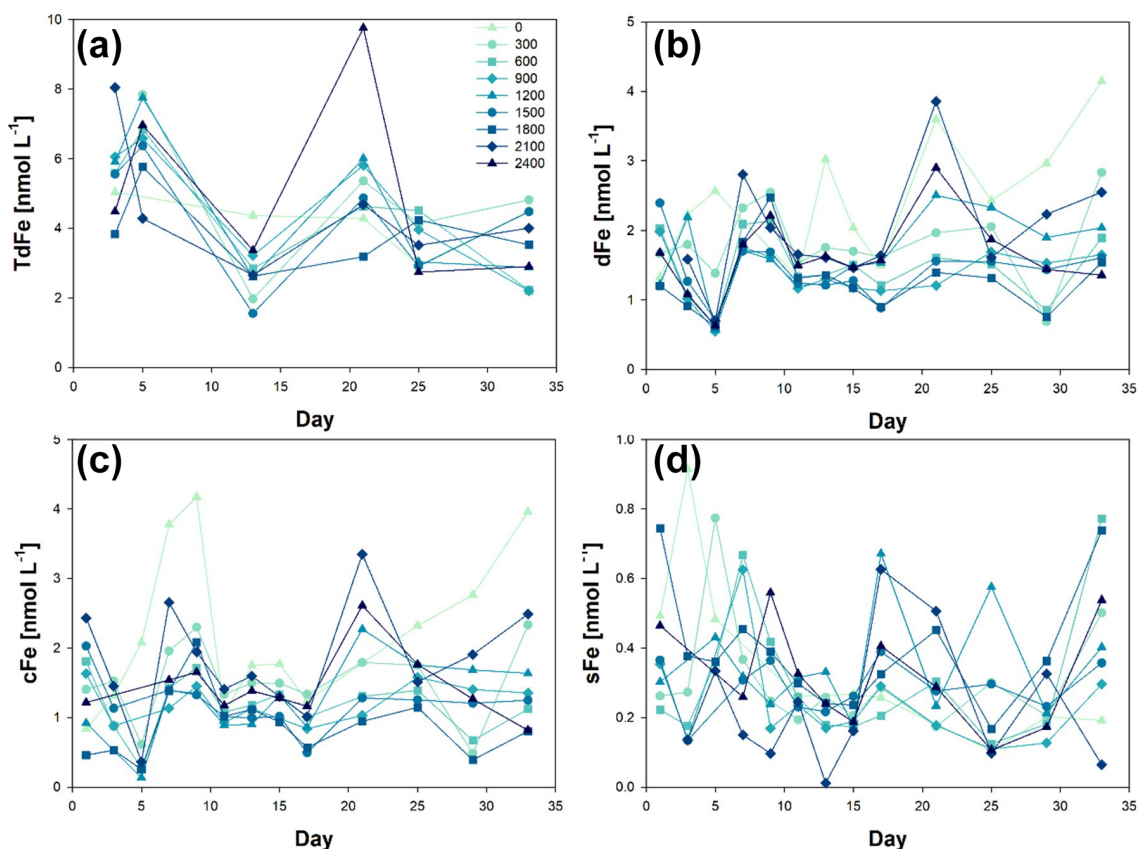


Figure 2. Temporal evolution of (a) total dissolvable iron (TdFe), (b) dissolved iron (dFe), (c) colloidal iron ($cFe = dFe - sFe$), and (d) soluble iron (sFe) concentrations from day 0 to day 33 of the mesocosm experiment for the nine increased alkalinity mesocosms ranging from 0 (light blue) to $2400 \mu\text{mol L}^{-1}$ (dark blue). Symbols and colour codes as in Fig. 1c. The concentration range of the different size fractions is different. Three y-axis ranges have been used: up to 10 nmol L^{-1} for TdFe, up to 5 nM for dFe and cFe, and up to 1 nmol L^{-1} for sFe.

cium carbonate precipitation and dissolution (Segovia et al., 2017). These processes were highly active during our experiment, especially during Phase II (Paul et al., 2024; Marin-Samper et al., 2024), thus probably directly affecting metal speciation.

The mesocosm with $\Delta 2100$ was not included in the calculated means due to an outlier in both $dFe = 5.30 \pm 0.10$ and $sFe = 2.86 \pm 0.05 \text{ nmol L}^{-1}$. The first TdFe samples were taken on day t3 and averaged $6.26 \pm 2.4 \text{ nmol L}^{-1}$. The high standard deviation in the results was caused by $\Delta 300$ and $\Delta 2100$. When these two mesocosms were excluded, the average concentration decreased to $5.21 \pm 0.81 \text{ nmol L}^{-1}$.

On day t4, sodium carbonate salts, NaHCO_3 and Na_2CO_3 , were added to the mesocosms and Phase II started. Mesocosms in which ΔTA was greater than $300 \mu\text{mol L}^{-1}$ showed decreases in dFe. The resulting dFe concentrations were $0.63 \pm 0.06 \text{ nmol L}^{-1}$ for all the mesocosms except for ΔTA 0 and $300 \mu\text{mol L}^{-1}$ (2.56 ± 0.02 and $1.39 \pm 0.08 \text{ nmol L}^{-1}$, respectively). These concentrations were the lowest observed throughout all the experiment and showed the least variation between mesocosms at any time point. The decrease in dFe

was most likely caused by a decrease in colloidal sized Fe (cFe). Aggregation processes did not affect the sFe, which remained relatively unchanged. Mesocosms 5 and 1 (ΔTA 0 and $300 \mu\text{mol L}^{-1}$ respectively) showed higher concentrations but were within the analysis range observed during the mesocosm experiments.

Two days after the alkalization event, dFe concentrations returned to the original concentration range ($2.00 \pm 0.39 \text{ nmol L}^{-1}$). This change in concentration back to normal did not correlate with the addition of NaHCO_3 and Na_2CO_3 required for the OAE. The increase in dFe was not accompanied by an increase in sFe along Phase I. It was the cFe fraction that varied. This suggests that aggregation processes of colloidal particles occurred with other particles with limited adsorption/absorption of sFe. TdFe also increased after the addition of NaHCO_3 and Na_2CO_3 . This increase could be due to multiple reasons including (1) the opening of the mesocosms, which could have allowed for aerial input of iron; (2) the addition of Fe during the addition of NaHCO_3 and Na_2CO_3 including possible trace amounts in the used reagents; (3) the lack of trace metal clean con-

ditions; (4) the presence of mesozooplankton faecal pellets; and (5) the aggregation of cFe and dFe could have led to the formation of larger size particles (> 0.2 mm) that could have been dissolved during the 6 months of sample acidification, compared to highly refractory particles that may not solubilize in 2% *v/v* HCl.

This mesocosm experiment was carried out in coastal waters where Fe is not a limiting micronutrient (López-García et al., 2021; Arnone et al., 2022). However, Fe redox processes should be considered in future OAE where iron can become a limiting element. For example, Fe(II) is considered the most bioavailable Fe species as it is less energetically costly to uptake by organisms. However, in the current oxic ocean, Fe(II) is rapidly oxidized to Fe(III) (Santana-Casiano et al., 2005). The addition of NaHCO_3 and Na_2CO_3 reduced the cFe concentration. Recent studies of Fe(II) oxidation kinetics have shown that colloidal size particles play a significant role in Fe(II) oxidation kinetics (González-Santana et al., 2021). Indeed, a decrease in colloids drastically accelerates the Fe(II) oxidation rate, which subsequently could lead to a decrease in available Fe(II), reducing Fe bioavailability and Fe acquisition costs in terms of energy (microbial/enzymatic catalysis) (Fujii et al., 2010; Anderson and Morel, 1982).

Correlations between the different iron size fractions and their ratios, mesocosm physico-chemical parameters (i.e. pH, alkalinity, dissolved inorganic carbon, nitrates, nitrites, silicates), and biological variables (i.e. fluorescence, community respiration, net primary production, pico- and nanoeukaryote concentration) did not present any statistical significance (Fig. S3). Initial statistical tests showed a significant inverse correlation ($p < 0.05$ and $r > -0.5$) between TdFe and DIC and TA; however, when further tests were performed for Phase II, correlation decreased ($p > 0.28$ and $r = -0.15$). These results show that iron concentrations were not limiting during the experiments, and so any of the phytoplankton functional groups were below their Fe demand for growth (Segovia et al., 2017). This is a direct result of high iron concentration as a consequence of the study site being located in coastal waters with high Fe inputs such as sediment re-suspension in coastal waters and aerial inputs due to the Canary Islands location, which would increase initial Fe concentrations used in the mesocosms compared to open ocean locations. Yet, such Fe concentrations were not toxic either, since phytoplankton growth was not hampered in Phase II. In fact, the contrary occurred, and chlorophyll *a* (Chl *a*) levels increased in parallel with a significant recovery in the F_v/F_m ratio (Ramírez et al., 2024). These improvements in Chl *a* and photophysiology data are primarily attributed to the emergence of blooms of large nanoeukaryotes and picoeukaryotes in $\Delta 1500$, $\Delta 1800$, $\Delta 600$, and $\Delta 900$ at t27.

In light of this, we suggest that iron size fractions and phytoplankton are independent. However, we have more than a reasonable doubt about the colloidal fraction being directly linked with mesozooplankton faecal pellets. For instance, $> 200\%$ of a mixture of lithogenic and biogenic Fe

seems to be egested via Antarctic mesozooplankton faecal pellets, while only 5% of the body iron content is assimilated (Schmidt et al., 2016; Cabanes et al., 2017). In any case, more work is needed to clarify this particular point.

3.2 Iron ligand distribution

Considering that the OAEs were not carried out under trace metal clean conditions, according to the GEOTRACES protocol (Cutter et al., 2017), except for both sample collection and measurement in the ULPGC facilities, the OAE experiments have demonstrated non-linearity in the behaviour of Fe-binding ligands (L_{Fe}) and the conditional stability constant ($\log K_{\text{Fe'L}}^{\text{cond}}$) across the entire alkalinity gradient (Fig. 3). Fe-binding ligands in the ocean come from different sources such as rupture of cells after grazing (Sato et al., 2007), viral lysis (Poorvin et al., 2011), transformation of organic matter (Gerringa et al., 2006), phytoplankton exudates (Rico et al., 2013; Santana-Casiano et al., 2014), and sediments (Gerringa et al., 2008). The L_{Fe} are classified according to the value of the conditional stability constants ($\log K_{\text{Fe'L}}^{\text{cond}}$). These ligands can be considered to be strong (L_1) or weak (L_2), where $\log K_{\text{Fe'L}}^{\text{cond}} = 12$ divides L_1 and L_2 type of Fe-binding ligands (Gledhill and Buck, 2012).

Specifically, before OAE (Phase 0), L_{Fe} concentrations ranged from 6.81 nmol L^{-1} ($\Delta 300$) to 1.51 nmol L^{-1} ($\Delta 1800$). Throughout the course of the experiments, the mean L_{Fe} concentration across all mesocosms was $4.14 \pm 2.01 \text{ nmol L}^{-1}$, with a $\log K_{\text{Fe'L}}^{\text{cond}}$ value of 11.63 ± 0.36 , being L_2 class in most of the cases (90.5% of the 84 data). Notably, there was a discernible alteration in the behaviour of L_{Fe} in the $\Delta 1500$ mesocosm, coincident with the emergence of blooms of the haptophyte *Chrysochromulina tobinii* at t27 (Marín-Samper et al., 2024). L_{Fe} consistently exhibited higher concentrations than dFe, with the exception of mesocosm $\Delta 2100$ at t1, $\Delta 900$ at t5, $\Delta 600$ at t5 and t27, $\Delta 2400$ at t5, and $\Delta 1200$ at t3 and t5. In these instances, the titration curves were linear, suggesting oversaturation of the natural ligands with the Fe content. Consequently, the percentage of Fe organically complexed (% FeL) was determined to be 99.8 ± 0.2 . The concentration of labile Fe (Fe') was in the range from 0.04 to $15.98 \text{ pmol L}^{-1}$, and Fe^{3+} species, primarily $\text{Fe}(\text{OH})_3$, was calculated to be within the concentration range of 1.6×10^{-21} to $3.9 \times 10^{-26} \text{ mol L}^{-1}$.

It is important to remark that the experiment was not conducted under trace metal clean conditions. Consequently, discussing the potential Fe limitation in relation to the measured concentrations becomes a complex task. Additionally, the possibility of Fe contamination during the sampling process for other variables, which may influence Fe concentration and Fe-binding ligands, cannot be definitively ruled out.

The initial concentrations of dFe and L_{Fe} at the start of the experiments were found to be higher than those observed in coastal waters previously documented by Arnone

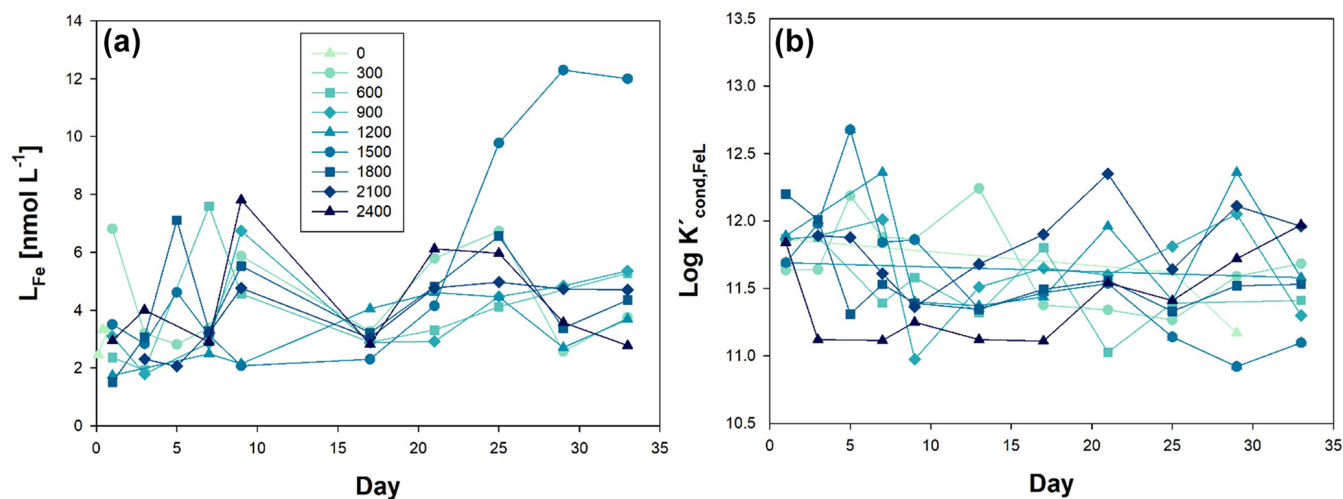


Figure 3. Temporal evolution of (a) iron ligands (L_{Fe}), and (b) conditional constant (K_{cond}), from day 0 to day 33 of the mesocosm experiment for the nine increased alkalinity mesocosms ranging from 0 (light blue) to 2400 $\mu\text{mol L}^{-1}$ (dark blue). Symbols and colour codes as in Fig. 1c.

et al. (2022) in the Canary Islands. Specifically, the mean dFe concentration in the region was determined to be $0.80 \pm 0.16 \text{ nmol L}^{-1}$, with corresponding mean L_{Fe} levels of $1.28 \pm 0.21 \text{ nmol L}^{-1}$. The initial L_{Fe} concentrations within the OAE mesocosms ranged from 1.51 to 6.81 nmol L^{-1} , and their evolution over time fell within the range of 1.51 to $12.30 \text{ nmol L}^{-1}$. These values were also in line with data from surface waters of the Atlantic Ocean, ranging from 0.1 to 0.8 nmol L^{-1} (Boye et al., 2006; Rijkenberg et al., 2008). The pumping of more coastal water to fill the mesocosms could explain the observed increase in concentrations.

Measurement of L_{Fe} within the mesocosms indicated a consistent nature of Fe-binding ligands, as reflected by the comparable values of the $\log K_{Fe'L}^{cond}$ throughout the entire study period, within the range of 10.91–12.68, corresponding to the L_2 and L_1 class, being weaker ligands (L_2) more abundant than stronger ligands (L_1), representing 90.5 % of the samples. In the surrounding waters of the Canary Islands, $\log K_{Fe'L}^{cond}$ values were reported to range between 10.77 and 11.90 (with a mean value of 11.45 ± 0.29) (Arnone et al., 2022), aligning with surface ocean waters in the region ($\log K_{Fe'L}^{cond}$ 8.8–12.85) (Boye et al., 2006; Bundy et al., 2015; Rijkenberg et al., 2008; Thuróczy et al., 2010; Boye et al., 2003).

The ratio of L_{Fe} to dFe serves as an indicator of the saturation state of ligands and whether conditions favour precipitation (Thuróczy et al., 2011). The observation of an excess of L_{Fe} with values exceeding 1 nmol L^{-1} may suggest biological production of ligands. Thuróczy et al. (2011) previously reported a ratio of approximately 4.4 for surface waters characterized by high phytoplankton activity. In the case of our OAE experiment, the production of Fe-binding lig-

ands may be attributed to the increase in large nanoplankton and microplankton biomass as described by Ramírez et al. (2024) during Phase II, which was specially observable in the $\Delta 1500$ treatment. Additionally, the presence of cyanobacteria, during the OAE can lead to the production of siderophores, as indicated by $\log K_{Fe'L}^{cond}$ values falling between 11 and 14 (Bundy et al., 2018; Witter et al., 2000). Siderophores are organic molecules of microbial origin that bind metals with different affinities. They are thought to play an important role in iron cycling in the ocean, but relatively few marine siderophores have been identified. Recently, new siderophores produced by *Synechococcus* sp. PCC 7002 have been discovered and characterized (Boiteau and Repeta, 2015), which is of relevance considering that *Synechococcus* spp. peaked during Phase II.

Furthermore, other types of ligands, such as polyphenolic compounds, may also be present, consistent with their $\log K_{Fe'L}^{cond}$ values (Arreguin et al., 2021; González et al., 2019). Weak Fe-binding ligands ($\log K_{Fe'L}^{cond} < 12$) could potentially be produced during the grazing of phytoplankton and the bacterial remineralization of sinking organic particles (Poorvin et al., 2011; Sato et al., 2007).

The observed variability in labile Fe concentrations (Fe') within the range of 0.04 to $15.98 \text{ pmol L}^{-1}$ aligns with the findings of Arnone et al. (2022). Notably, the limited concentration of Fe^{3+} precludes the favoured precipitation of iron hydroxides. It has been established that the presence of organic binding ligands enhances the solubility of Fe, as demonstrated by previous research (Liu and Millero, 2002; Segovia et al., 2017).

Similar to iron size fraction concentrations, L_{Fe} and $K_{Fe'L}^{cond}$ did not present any statistical correlation with any other measured physico-chemical or biological parameter. This sug-

gests that the alkalinity addition in the mesocosm experiments did not affect the Fe concentration, fractionation, and speciation.

This OAE experiment was based on the addition of sodium carbonate salts. However, one might wonder what the pros and cons of this method are in comparison to other weathering-based carbon dioxide removal (CDR) techniques. For instance, similar alkalinity concentrations could have been obtained by adding calcium or magnesium carbonate salts. However, a previous study showed that the addition of calcium or magnesium salts would have led to changes in the iron speciation (Santana-Casiano et al., 2010). Also open ocean dissolution of the iron-containing mineral olivine was simulated by using a marine carbon cycle model (Hauck et al., 2016). They found that after equilibration with the atmosphere, the addition of olivine did not compensate enough for the effect of ocean acidification, and, in the real-world experiments, olivine-prompted silicic acid and iron fertilization might have undesired effects since increased dFe does not always have beneficial consequences for the community (Coale, 1991; Behrenfeld and Milligan, 2013).

4 Conclusions

The OAE experiments, while not conducted under stringent trace metal conditions according to the GEOTRACES protocol, have provided valuable insights into the non-linear behaviour of Fe-binding ligands (L_{Fe}) and the conditional stability constant ($\log K_{\text{Fe}^{\text{L}}}^{\text{cond}}$) across the entire alkalinity gradient. L_{Fe} concentrations increased 2-fold just after OAE with a $\log K_{\text{Fe}^{\text{L}}}^{\text{cond}}$ throughout within the range of 10.91–12.68. This suggests the possible biological production of ligands, particularly during the emergence of nanoeukaryotes blooms and peaks of *Synechococcus* in the $\Delta 1500$ treatment, as well as zooplankton grazing. Similarly, dFe concentrations were higher than those one might expect in the Macaronesia region. This could have been a result of the manipulation required to fill in mesocosms in the open environment, where the iron sources such as sediment resuspension, aerial input, and water runoffs are combined with our mesocosm manipulation. During the OAE we did not observe any iron size fractionation changes and concentration variations due to different OAE conditions. Nevertheless, the addition of sodium carbonate salts (NaHCO_3 and Na_2CO_3) coincided with a decrease in the dFe concentration just after the addition. However, concentrations returned to background level concentrations in 48 h. Soluble iron remained below 0.8 nmol L^{-1} through the whole experiment and did not change after the sodium carbonate salt addition. The results suggest that the added sodium carbonate salts may affect cFe but quickly return to the original concentrations in coastal waters. Nevertheless, the observable decrease is not proportional to the increase in alkalinity, where other factors such as aggregation

due to increases in particles or added mineral salts produce a short-term cFe decrease.

The iron size fractionation, concentration, and iron-binding ligand data support the fact that the addition of sodium salts in this mesocosm experiment did not lead to significant changes in the iron cycle; therefore phytoplankton were not affected by changes in this essential element. This may have wider environmental implications in large-scale experiments and implementation of CDRs in larger ocean. However, it is important to consider that while employing this oceanic iron fertilization (OAE) technique in coastal waters might not significantly impact the iron cycle, outcomes could differ under varying conditions. For instance, if the experiment were conducted in oligotrophic open ocean waters, the presence of a bloom exceeding those observed in these experiments could lead to different results. Conversely, an excess of iron might inhibit phytoplankton growth due to potential toxic effects. Therefore, further research into the effects of carbon dioxide removal (CDR) techniques on trace metals is essential to mitigate unintended consequences on the ecosystem.

Data availability. The raw data supporting the conclusions of this article will be made available by the authors upon request.

Supplement. The supplement related to this article is available online at: <https://doi.org/10.5194/bg-21-2705-2024-supplement>.

Author contributions. Experimental concept and design: UR and JA (IOCAG). Execution of the experiment: all authors. Data analysis: DGS, AGG, MGD, and JMSC. Manuscript preparation: DGS. Manuscript revisions: all authors.

Competing interests. The contact author has declared that none of the authors has any competing interests.

Disclaimer. Publisher's note: Copernicus Publications remains neutral with regard to jurisdictional claims made in the text, published maps, institutional affiliations, or any other geographical representation in this paper. While Copernicus Publications makes every effort to include appropriate place names, the final responsibility lies with the authors.

Special issue statement. This article is part of the special issue "Environmental impacts of ocean alkalinity enhancement". It is not associated with a conference.

Acknowledgements. We would like to thank the Oceanic Platform of the Canary Islands (PLOCAN) and its staff for the use of their fa-

cilities and for their help with the logistics and organization of this experiment. We are also grateful to Andrea Ludwig and Jana Meyer (KOSMOS Logistics and Coordination), to Jan Hennke, Michael Krudewig, and Anton Theileis (KOSMOS technical staff), and to Michael Sswat, Carsten Spisla, Daniel Brüggemann, Silvan Goldenberg, Joaquin Ortiz, Nicolás Sánchez, and Philipp Suessele (KOSMOS Scientific Diving and Maintenance Team).

Financial support. This research has been supported by the Ocean-NETS project (“Ocean-based Negative Emissions Technologies – analysing the feasibility, risks and co-benefits of ocean-based negative emission technologies for stabilizing the climate”, EU Horizon 2020 Research and Innovation Programme grant agreement no. 869357) and the Helmholtz European Partnering project Ocean-CDR (“Ocean-based carbon dioxide removal strategies”, project no. PIE-0021) with additional support from the AQUACOSM-plus project (EU H2020-INFRAIA project no. 871081, “AQUACOSM-plus: Network of Leading European AQUATIC MesoCOSM Facilities Connecting Rivers, Lakes, Estuaries and Oceans in Europe and beyond”).

Review statement. This paper was edited by Jaime Palter and reviewed by two anonymous referees.

References

- Anderson, M. A. and Morel, F. M. M.: The influence of aqueous iron chemistry on the uptake of iron by the coastal diatom *Thalassiosira weissflogii*, *Limnol. Oceanogr.*, 27, 789–813, <https://doi.org/10.4319/lo.1982.27.5.0789>, 1982.
- Arnone, V., González-Santana, D., González-Dávila, M., González, A. G., and Santana-Casiano, J. M.: Iron and copper complexation in Macaronesian coastal waters, *Mar. Chem.*, 240, 104087, <https://doi.org/10.1016/J.MARCHEM.2022.104087>, 2022.
- Arreguin, M. L., González, A. G., Pérez-Almeida, N., Arnone, V., González-Dávila, M., and Santana-Casiano, J. M.: The role of gentisic acid on the Fe(III) redox chemistry in marine environments, *Mar. Chem.*, 234, 104003, <https://doi.org/10.1016/J.MARCHEM.2021.104003>, 2021.
- Bach, L. T., Gill, S. J., Rickaby, R. E. M., Gore, S., and Renforth, P.: CO₂ Removal With Enhanced Weathering and Ocean Alkalinity Enhancement: Potential Risks and Co-benefits for Marine Pelagic Ecosystems, *Front. Clim.*, 1, 476698, <https://doi.org/10.3389/FCLIM.2019.00007/BIBTEX>, 2019.
- Barbeau, K.: Photochemistry of Organic Iron(III) Complexing Ligands in Oceanic Systems, *Photochem. Photobiol.*, 82, 1505–1516, <https://doi.org/10.1111/j.1751-1097.2006.tb09806.x>, 2006.
- Behrenfeld, M. J. and Milligan, A. J.: Photophysiological Expressions of Iron Stress in Phytoplankton, *Ann. Rev. Mar. Sci.*, 5, 217–246, <https://doi.org/10.1146/annurev-marine-121211-172356>, 2013.
- Benner, R.: Loose ligands and available iron in the ocean, *P. Natl. Acad. Sci. USA*, 108, 893–894, <https://doi.org/10.1073/pnas.1018163108>, 2011.
- Boiteau, R. M. and Repeta, D. J.: An extended siderophore suite from *Synechococcus* sp. PCC 7002 revealed by LC-ICPMS-ESIMS, *Metallomics*, 7, 877–884, <https://doi.org/10.1039/c5mt00005j>, 2015.
- Boyd, P. W. and Ellwood, M. J.: The biogeochemical cycle of iron in the ocean, *Nat. Geosci.*, 3, 675–682, <https://doi.org/10.1038/ngeo964>, 2010.
- Boye, M., Aldrich, A. P., van den Berg, C. M. G., de Jong, J. T. M., Veldhuis, M., and de Baar, H. J. W.: Horizontal gradient of the chemical speciation of iron in surface waters of the northeast Atlantic Ocean, *Mar. Chem.*, 80, 129–143, [https://doi.org/10.1016/S0304-4203\(02\)00102-0](https://doi.org/10.1016/S0304-4203(02)00102-0), 2003.
- Boye, M., Aldrich, A., van den Berg, C. M. G., de Jong, J. T. M., Nirmaier, H., Veldhuis, M. J. W., Timmermans, K. R., and de Baar, H. J. W.: The chemical speciation of iron in the north-east Atlantic Ocean, *Deep-Sea Res. Pt. I*, 53, 667–683, <https://doi.org/10.1016/j.dsr.2005.12.015>, 2006.
- Bundy, R. M., Abdulla, H. A. N., Hatcher, P. G., Biller, D. V., Buck, K. N., and Barbeau, K. A.: Iron-binding ligands and humic substances in the San Francisco Bay estuary and estuarine-influenced shelf regions of coastal California, *Mar. Chem.*, 173, 183–194, 2015.
- Bundy, R. M., Boiteau, R. M., McLean, C., Turk-Kubo, K. A., McIlvin, M. R., Saito, M. A., Van Mooy, B. A. S., and Repeta, D. J.: Distinct Siderophores Contribute to Iron Cycling in the Mesopelagic at Station ALOHA, <https://www.frontiersin.org/articles/10.3389/fmars.2018.00061> (last access: 6 May 2024), 2018.
- Cabanes, D. J. E., Norman, L., Santos-Echeandía, J., Iversen, M. H., Trimborn, S., Laglera, L. M., and Hassler, C. S.: First evaluation of the role of salp fecal pellets on iron biogeochemistry, *Front. Mar. Sci.*, 3, 289, <https://doi.org/10.3389/fmars.2016.00289>, 2017.
- Campos, M. L. A. and van den Berg, C. M.: Determination of copper complexation in sea water by cathodic stripping voltammetry and ligand competition with salicylaldehyde, *Anal. Chim. Acta*, 284, 481–496, [https://doi.org/10.1016/0003-2670\(94\)85055-0](https://doi.org/10.1016/0003-2670(94)85055-0), 1994.
- Coale, K. H.: Effects of iron, manganese, copper, and zinc enrichments on productivity and biomass in the subarctic Pacific, *Limnol. Oceanogr.*, 36, 1851–1864, <https://doi.org/10.4319/lo.1991.36.8.1851>, 1991.
- Colbourn, G., Ridgwell, A., and Lenton, T. M.: The time scale of the silicate weathering negative feedback on atmospheric CO₂, *Global Biogeochem. Cy.*, 29, 583–596, <https://doi.org/10.1002/2014GB005054>, 2015.
- Croot, P. L. and Johansson, M.: Determination of Iron Speciation by Cathodic Stripping Voltammetry in Seawater Using the Competing Ligand 2-(2-Thiazolylazo)-p-cresol (TAC), *Electroanalysis*, 12, 565–576, [https://doi.org/10.1002/\(SICI\)1521-4109\(200005\)12:8<565::AID-ELAN565>3.0.CO;2-L](https://doi.org/10.1002/(SICI)1521-4109(200005)12:8<565::AID-ELAN565>3.0.CO;2-L), 2000.
- Cutter, G. A., Casciotti, K., Croot, P., Geibert, W., Heimbürger, L.-E., Lohan, M. C., Planquette, H., and van de Fliedert, T.: Sampling and sample-handling protocols for GEOTRACES Cruises, Version 3.0, <https://www.geotraces.org/methods-cookbook/> (last access: 15 May 2024), 2017.
- Feng, E. Y., Keller, D. P., Koeve, W., and Oschlies, A.: Could artificial ocean alkalization protect tropical coral ecosystems?

- tems from ocean acidification?, *Environ. Res. Lett.*, 11, 74008, <https://doi.org/10.1088/1748-9326/11/7/074008>, 2016.
- Fujii, M., Rose, A. L., Omura, T., and Waite, T. D.: Effect of Fe(II) and Fe(III) Transformation Kinetics on Iron Acquisition by a Toxic Strain of *Microcystis aeruginosa*, *Environ. Sci. Technol.*, 44, 1980–1986, <https://doi.org/10.1021/es901315a>, 2010.
- Gerringa, L. J. A., Veldhuis, M. J. W., Timmermans, K. R., Sarthou, G., and de Baar, H. J. W.: Co-variance of dissolved Fe-binding ligands with phytoplankton characteristics in the Canary Basin, *Mar. Chem.*, 102, 276–290, <https://doi.org/10.1016/j.marchem.2006.05.004>, 2006.
- Gerringa, L. J. A., Blain, S., Laan, P., Sarthou, G., Veldhuis, M. J. W., Brussaard, C. P. D., Viollier, E., and Timmermans, K. R.: Fe-binding dissolved organic ligands near the Kerguelen Archipelago in the Southern Ocean (Indian sector), *Deep-Sea Res. Pt. II*, 55, 606–621, <https://doi.org/10.1016/j.dsr2.2007.12.007>, 2008.
- Gledhill, M. and Buck, K. N.: The Organic Complexation of Iron in the Marine Environment: A Review, *Front. Microbiol.*, 69, 3, <https://doi.org/10.3389/fmicb.2012.00069>, 2012.
- González, A. G., Cadena-Aizaga, M. I., Sarthou, G., González-Dávila, M., and Santana-Casiano, J. M.: Iron complexation by phenolic ligands in seawater, *Chem. Geol.*, 511, 380–388, <https://doi.org/10.1016/j.chemgeo.2018.10.017>, 2019.
- González-Dávila, M., Santana-Casiano, J. M., and Millero, F. J.: Competition between O₂ and H₂O₂ in the oxidation of Fe(II) in natural waters, *J. Solut. Chem.*, 35, 95–111, <https://doi.org/10.1007/s10953-006-8942-3>, 2006.
- González-Santana, D., González-Dávila, M., Lohan, M. C., Artigue, L., Planquette, H., Sarthou, G., Tagliabue, A., and Santana-Casiano, J. M.: Variability in iron (II) oxidation kinetics across diverse hydrothermal sites on the northern Mid Atlantic Ridge, *Geochim. Cosmochim. Ac.*, 297, 143–157, <https://doi.org/10.1016/j.gca.2021.01.013>, 2021.
- Guo, J. A., Strzepek, R., Willis, A., Ferderer, A., and Bach, L. T.: Investigating the effect of nickel concentration on phytoplankton growth to assess potential side-effects of ocean alkalinity enhancement, *Biogeosciences*, 19, 3683–3697, <https://doi.org/10.5194/bg-19-3683-2022>, 2022.
- Hartmann, J., West, A. J., Renforth, P., Köhler, P., De La Rocha, C. L., Wolf-Gladrow, D. A., Dürr, H. H., and Scheffran, J.: Enhanced chemical weathering as a geoengineering strategy to reduce atmospheric carbon dioxide, supply nutrients, and mitigate ocean acidification, *Rev. Geophys.*, 51, 113–149, <https://doi.org/10.1002/rog.20004>, 2013.
- Hauck, J., Köhler, P., Wolf-Gladrow, D., and Völker, C.: Iron fertilisation and century-scale effects of open ocean dissolution of olivine in a simulated CO₂ removal experiment, *Environ. Res. Lett.*, 11, 24007, <https://doi.org/10.1088/1748-9326/11/2/024007>, 2016.
- Hopkinson, B. M. and Barbeau, K. A.: Organic and redox speciation of iron in the eastern tropical North Pacific suboxic zone, *Mar. Chem.*, 106, 2–17, <https://doi.org/10.1016/j.marchem.2006.02.008>, 2007.
- Jickells, T. D., An, Z. S., Andersen, K. K., Baker, A. R., Bergametti, C., Brooks, N., Cao, J. J., Boyd, P. W., Duce, R. A., Hunter, K. A., Kawahata, H., Kubilay, N., LaRoche, J., Liss, P. S., Mahowald, N. M., Prospero, J. M., Ridgwell, A. J., Tegen, I., and Torres, R.: Global iron connections between desert dust, ocean biogeochemistry, and climate, *Science*, 308, 67–71, <https://doi.org/10.1126/science.1105959>, 2005.
- Kheshgi, H. S.: Sequestering atmospheric carbon dioxide by increasing ocean alkalinity, *Energy*, 20, 915–922, [https://doi.org/10.1016/0360-5442\(95\)00035-F](https://doi.org/10.1016/0360-5442(95)00035-F), 1995.
- Lenton, A., Matear, R. J., Keller, D. P., Scott, V., and Vaughan, N. E.: Assessing carbon dioxide removal through global and regional ocean alkalization under high and low emission pathways, *Earth Syst. Dynam.*, 9, 339–357, <https://doi.org/10.5194/esd-9-339-2018>, 2018.
- Liu, X. and Millero, F. J.: The solubility of iron in seawater, *Mar. Chem.*, 77, 43–54, [https://doi.org/10.1016/S0304-4203\(01\)00074-3](https://doi.org/10.1016/S0304-4203(01)00074-3), 2002.
- Lohan, M. C., Aguilar-Islas, A. M., and Bruland, K. W.: Direct determination of iron in acidified (pH 1.7) seawater samples by flow injection analysis with catalytic spectrophotometric detection: Application and intercomparison, *Limnol. Oceanogr. Method.*, 4, 164–171, <https://doi.org/10.4319/lom.2006.4.164>, 2006.
- López-García, P., Gelado-Caballero, M. D., Patey, M. D., and Hernández-Brito, J. J.: Atmospheric fluxes of soluble nutrients and Fe: More than three years of wet and dry deposition measurements at Gran Canaria (Canary Islands), *Atmos. Environ.*, 246, 118090, <https://doi.org/10.1016/j.atmosenv.2020.118090>, 2021.
- Lorenzo, M. R., Segovia, M., Cullen, J. T., and Maldonado, M. T.: Particulate trace metal dynamics in response to increased CO₂ and iron availability in a coastal mesocosm experiment, *Biogeosciences*, 17, 757–770, <https://doi.org/10.5194/bg-17-757-2020>, 2020.
- Marín-Samper, L., Arístegui, J., Hernández-Hernández, N., Ortiz, J., Archer, S. D., Ludwig, A., and Riebesell, U.: Assessing the impact of CO₂ equilibrated ocean alkalinity enhancement on microbial metabolic rates in an oligotrophic system, *EGU sphere* [preprint], <https://doi.org/10.5194/egusphere-2023-2409>, 2023.
- Mausz, M. A., Segovia, M., Larsen, A., Berger, S. A., Egge, J. K., and Pohnert, G.: High CO₂ concentration and iron availability determine the metabolic inventory in an *Emiliania huxleyi*-dominated phytoplankton community, *Environ. Microbiol.*, 22, 3863–3882, <https://doi.org/10.1111/1462-2920.15160>, 2020.
- Millero, F. J., Woosley, R., Dittrolo, B., and Waters, J.: Effect of Ocean Acidification on the Speciation of Metals in Seawater, *Oceanography*, 22, 72–85, 2009.
- Moffett, J. W.: Iron(II) in the world's oxygen deficient zones, *Chem. Geol.*, 580, 120314, <https://doi.org/10.1016/j.chemgeo.2021.120314>, 2021.
- Moore, J. K., Doney, S. C., Glover, D. M., and Fung, I. Y.: Iron cycling and nutrient-limitation patterns in surface waters of the World Ocean, *Deep-Sea Res. Pt. II*, 49, 463–507, [https://doi.org/10.1016/S0967-0645\(01\)00109-6](https://doi.org/10.1016/S0967-0645(01)00109-6), 2001.
- Obata, H., Karatani, H., and Nakayama, E.: Automated Determination of Iron in Seawater by Chelating Resin Concentration and Chemiluminescence Detection, *Anal. Chem.*, 65, 1524–1528, <https://doi.org/10.1021/ac00059a007>, 1993.
- Omanović, D., Garnier, C., and Pižeta, I.: ProMCC: An all-in-one tool for trace metal complexation studies, *Mar. Chem.*, 173, 25–39, <https://doi.org/10.1016/j.marchem.2014.10.011>, 2015.
- Paul, A. J., Haunost, M., Goldenberg, S. U., Hartmann, J., Sánchez, N., Schneider, J., Suitner, N., and Riebesell, U.: Ocean alkalinity enhancement in an open ocean ecosystem: Biogeochemical

- responses and carbon storage durability, *EGUsphere* [preprint], <https://doi.org/10.5194/egusphere-2024-417>, 2024.
- Poorvin, L., Sander, S. G., Velasquez, I., Ibisami, E., LeClerc, G. R., and Wilhelm, S. W.: A comparison of Fe bioavailability and binding of a catecholate siderophore with virus-mediated lysates from the marine bacterium *Vibrio alginolyticus* PWH3a, *J. Exp. Mar. Biol. Ecol.*, 399, 43–47, <https://doi.org/10.1016/j.jembe.2011.01.016>, 2011.
- Ramírez, L., Pozzo-Pirotta, L. J., Trebec, A., Manzanares-Vázquez, V., Díez, J. L., Aristegui, J., Riebesell, U., Archer, S. D., and Segovia, M.: Ocean Alkalinity Enhancement (OAE) does not cause cellular stress in a phytoplankton community of the sub-tropical Atlantic Ocean, *EGUsphere* [preprint], <https://doi.org/10.5194/egusphere-2024-847>, 2024.
- Renforth, P. and Henderson, G.: Assessing ocean alkalinity for carbon sequestration, *Rev. Geophys.*, 55, 636–674, <https://doi.org/10.1002/2016RG000533>, 2017.
- Rico, M., López, A., Santana-Casiano, J. M., González, A. G., and González-Dávila, M.: Variability of the phenolic profile in the diatom *Phaeodactylum tricornutum* growing under copper and iron stress, *Limnol. Oceanogr.*, 58, 144–152, <https://doi.org/10.4319/LO.2013.58.1.0144>, 2013.
- Riebesell, U., Czerny, J., von Bröckel, K., Boxhammer, T., Büdenbender, J., Deckelnick, M., Fischer, M., Hoffmann, D., Krug, S. A., Lentz, U., Ludwig, A., Mucche, R., and Schulz, K. G.: Technical Note: A mobile sea-going mesocosm system – new opportunities for ocean change research, *Biogeosciences*, 10, 1835–1847, <https://doi.org/10.5194/bg-10-1835-2013>, 2013.
- Rijkenberg, M. J. A., Powell, C. F., Dall’Osto, M., Nielsdotir, M. C., Patey, M. D., Hill, P. G., Baker, A. R., Jickells, T. D., Harrison, R. M., and Achterberg, E. P.: Changes in iron speciation following a Saharan dust event in the tropical North Atlantic Ocean, *Mar. Chem.*, 110, 56–67, <https://doi.org/10.1016/j.marchem.2008.02.006>, 2008.
- Santana-Casiano, J. M., González-Dávila, M., and Millero, F. J.: Oxidation of nanomolar level of Fe(II) with oxygen in natural waters, *Environ. Sci. Technol.*, 39, 2073–2079, <https://doi.org/10.1021/es049748y>, 2005.
- Santana-Casiano, J. M., González-Dávila, M., and Millero, F. J.: The role of Fe(II) species on the oxidation of Fe(II) in natural waters in the presence of O₂ and H₂O₂, *Mar. Chem.*, 99, 70–82, <https://doi.org/10.1016/j.marchem.2005.03.010>, 2006.
- Santana-Casiano, J. M., González-Dávila, M., González, A. G., and Millero, F. J.: Fe (III) reduction in the presence of catechol in seawater, *Aquat. Geochem.*, 16, 467–482, 2010.
- Santana-Casiano, J. M., González-Dávila, M., González, A. G., Rico, M., López, A., and Martel, A.: Characterization of phenolic exudates from *Phaeodactylum tricornutum* and their effects on the chemistry of Fe (II)–Fe (III), *Mar. Chem.*, 158, 10–16, 2014.
- Santana-Casiano, J. M., González-Santana, D., Devresse, Q., Hepach, H., Santana-González, C., Quack, B., Engel, A., and González-Dávila, M.: Exploring the Effects of Organic Matter Characteristics on Fe(II) Oxidation Kinetics in Coastal Seawater, *Environ. Sci. Technol.*, 56, 2718–2728, <https://doi.org/10.1021/acs.est.1c04512>, 2022.
- Sato, M., Takeda, S., and Furuya, K.: Iron regeneration and organic iron(III)-binding ligand production during in situ zooplankton grazing experiment, *Mar. Chem.*, 106, 471–488, <https://doi.org/10.1016/j.marchem.2007.05.001>, 2007.
- Schmidt, K., Schlosser, C., Atkinson, A., Fielding, S., Venables, H. J., Waluda, C. M., and Achterberg, E. P.: Zooplankton gut passage mobilizes lithogenic iron for ocean productivity, *Curr. Biol.*, 26, 2667–2673, 2016.
- Schulz, K. G. and Riebesell, U.: Diurnal changes in seawater carbonate chemistry speciation at increasing atmospheric carbon dioxide, *Mar. Biol.*, 160, 1889–1899, <https://doi.org/10.1007/s00227-012-1965-y>, 2013.
- Segovia, M., Lorenzo, M. R., Maldonado, M. T., Larsen, A., Berger, S. A., Tsagaraki, T. M., Lázaro, F. J., Iñiguez, C., García-Gómez, C., Palma, A., Mausz, M. A., Gordillo, F. J. L., Fernández, J. A., Ray, J. L., and Egge, J. K.: Iron availability modulates the effects of future CO₂ levels within the marine planktonic food web, *Mar. Ecol. Prog. Ser.*, 565, 17–33, 2017.
- Sutak, R., Camadro, J.-M., and Lesuisse, E.: Iron Uptake Mechanisms in Marine Phytoplankton, *Front. Microbiol.*, 11, 566691, <https://doi.org/10.3389/fmicb.2020.566691>, 2020.
- Tagliabue, A., Bowie, A. R., Boyd, P. W., Buck, K. N., Johnson, K. S., and Saito, M. A.: The integral role of iron in ocean biogeochemistry, *Nature*, 543, 51–59, <https://doi.org/10.1038/nature21058>, 2017.
- Taucher, J., Bach, L. T., Boxhammer, T., Nauendorf, A., Achterberg, E. P., Algueró-Muñiz, M., Aristegui, J., Czerny, J., Esposito, M., Guan, W., Haunost, M., Horn, H. G., Ludwig, A., Meyer, J., Spisla, C., Sswat, M., Stange, P., and Riebesell, U.: Influence of Ocean Acidification and Deep Water Upwelling on Oligotrophic Plankton Communities in the Subtropical North Atlantic: Insights from an In situ Mesocosm Study, *Front. Mar. Sci.*, 4, 85, <https://doi.org/10.3389/fmars.2017.00085>, 2017.
- Thuróczy, C.-E., Gerringa, L. J. A., Klunder, M. B., Middag, R., Laan, P., Timmermans, K. R., and de Baar, H. J. W.: Speciation of Fe in the Eastern North Atlantic Ocean, *Deep-Sea Res. Pt. I*, 57, 1444–1453, <https://doi.org/10.1016/j.dsr.2010.08.004>, 2010.
- Thuróczy, C.-E., Gerringa, L. J. A., Klunder, M. B., Laan, P., and de Baar, H. J. W.: Observation of consistent trends in the organic complexation of dissolved iron in the Atlantic sector of the Southern Ocean, *Deep-Sea Res. Pt. II*, 58, 2695–2706, <https://doi.org/10.1016/j.dsr2.2011.01.002>, 2011.
- Witter, A. E., Hutchins, D. A., Butler, A., and Luther, G. W.: Determination of conditional stability constants and kinetic constants for strong model Fe-binding ligands in seawater, *Mar. Chem.*, 69, 1–17, [https://doi.org/10.1016/S0304-4203\(99\)00087-0](https://doi.org/10.1016/S0304-4203(99)00087-0), 2000.
- Wu, J. and Luther III, G. W.: Size-fractionated iron concentrations in the water column of the western North Atlantic Ocean, *Limnol. Oceanogr.*, 39, 1119–1129, <https://doi.org/10.4319/lo.1994.39.5.1119>, 1994.
- Xin, X., Faucher, G., and Riebesell, U.: Phytoplankton response to increased nickel in the context of ocean alkalinity enhancement, *Biogeosciences*, 21, 761–772, <https://doi.org/10.5194/bg-21-761-2024>, 2024.
- Zeebe, R. E.: History of Seawater Carbonate Chemistry, Atmospheric CO₂, and Ocean Acidification, *Annu. Rev. Earth Pl. Sc.*, 40, 141–165, <https://doi.org/10.1146/annurev-earth-042711-105521>, 2012.